Supplementary Information:

Ni–N Interfacial Engineering Enables Noble-Metal-Free Ammonia Photodecomposition

Zhuohao Yang,[a] Md Sakib Hasan Khan,[a] Zhehao Sun,[a] Jiayi Chen,[a] Xuechen Jing,[a] Yi-Lun Chen,[b] Nicholas Cox,[a] Ary Wibowo,[b] Xiaolin Wang,[b] Rino Wu,[c] Daniel Macdonald,[b] Dongchen Qi,[c] Zongyou Yin*[a]

a. Research School of Chemistry, Australian National University, ACT 2601, Australia. E-mail: zongyou.yin@anu.edu.au
b. School of Engineering, Australian National University, Canberra, Australian Capital Territory 2601, Australia
c. School of Chemistry and Physics, Queensland University of Technology, Brisbane, Queensland 4001, Australia

Supporting methods

Chemicals preparation. TiO_2 **(**Sigma-Aldrich-Titanium (IV) oxide); $NiCl_2$ (Sigma-Aldrich-Nickle (II) chloride); Nitric acid (Sigma-Aldrich-ACS reagent, 70%); Formamide (Sigma-Aldrich-ACS reagent, ≥99.5%); DI water. All the chemical reagents were of analytical grade and used without any further purification.

Preparation of Ni-NC@TiO_2. Synthesis of Ni-NC@TiO_2 involves several steps. Initially, 200mg of TiO_2 is dispersed in 15 mL of formamide ($HCONH_2$) and stirred for 15 min until the solution is uniformly colored. Subsequently, 50, 100, 200mg of $NiCl_2$ is added to the solution and stirred for 3 h. Then, the mixture of 15 mL solution is transferred into a 50 mL autoclave for hydrothermal treatment at 180°C for 12 hours. Under these reaction conditions, formamide converts into amorphous nitrogen-doped carbon (NC) material. After the hydrothermal reaction, the material is washed 4 times with 1:1 ethanol and water, with centrifugation at 7800 revolutions per minute (rpm). The washed material is then treated with 0.1 mM dilute nitric acid 3 times, followed by water rinsing to remove the nitric acid. Subsequently, the material is dried in a vacuum oven at 60°C for 12 hours. The dried powder sample is ground and placed into a quartz boat, followed by annealing in an Ar environment in a tube furnace. The reaction temperature is set at 400°C for 4 hours with a heating rate of 5°C per min. Finally, the resulting samples (Ni-NC@TiO_2 (100mg)/-L (50mg)/-H (200mg)) are ground again to complete the synthesis process.

Preparation of NC@TiO_2. The synthesis steps for NC@TiO_2 are same as Ni-NC@TiO_2, except for adding $NiCl_2$.

Sample characterization

X-ray absorption spectroscopy (XAS) measurements were performed at the corresponding metal K-edge on the MEX-1 beamline at the Australian Synchrotron. All samples were finely ground, homogenised with high-purity cellulose, and diluted to an effective metal concentration of ~1000 ppm to minimise self-absorption effects. The resulting mixtures were pressed into 7 mm × 1 mm pellets and sealed between 8-μm Kapton films to prevent contamination and dehydration during measurement. XAS spectra were collected in fluorescence mode at room temperature under a continuous argon flow, which suppresses air scattering and prevents sample oxidation. Energy calibration was carried out simultaneously using the appropriate metal reference foil positioned downstream of the sample to ensure accurate alignment of the edge energies. Multiple scans were recorded for each sample and subsequently averaged to enhance the signal-to-noise ratio. Data reduction and analysis—including energy calibration, pre-edge subtraction, post-edge normalisation, and spline background fitting—were conducted using the ATHENA program within the Demeter software package.[1] X-ray photoelectron spectroscopy (XPS) was carried out using a Kratos AXIS Ultra DLD spectrometer with a monochromatic Al Kα source (hν = 1486.6 eV). Powder X-ray diffraction (XRD) patterns were recorded on a Bruker diffractometer using Cu Kα radiation. Gas products were analyzed by a Shimadzu Nexis GC-2030 equipped with a thermal conductivity detector (TCD) and a ShinCarbon column. Electron paramagnetic resonance (EPR) spectra were acquired on a Bruker E500 spectrometer equipped with a Bruker ER 4122 SHQE resonator. Micro-Raman spectroscopy was performed on a Horiba LabRAM system using a 532 nm diode-pumped solid-state laser and a Si CCD detector; the excitation power was kept constant for all measurements unless stated otherwise. Atomic force microscopy (AFM) data were collected using the Bruker Dimension Icon scanning probe microscope system with a SCANASYST-AIR tip.

Density functional theory (DFT) calculations

We atomistically modelled the TiO_2 (101) surface, N-doped C layer on top of it and Ni (011) nanoparticle exposed facet to reflect the HRTEM, XRD data in the model. The TiO_2 4x4 vacuum slab model was built first, then N-doped C was built as a shell layer. The Ni-nanoparticle six-atomic-cluster 011 surface was then built on the NC layer. The structures were geometrically relaxed under projected augmented wave (PAW) with conjugate gradient under Vienna Ab Initio Simulation Package (VASP). The PAW was incorporated to describe the interaction between valence electrons and ions. The Perdew-Burke-Erzerhof (PBE) functional was used to present exchange-correlation in the Kohn-Sham equation. The calculations were included the van der Waals (vdW) interaction under Grimme's DFT-D3 method. The plane-wave basis set with a kinetic energy cutoff of 500 eV was utilised. For the slabs, the 4 x 4 x 1 Mokhorst-Pack k-ponit grid matrix was implemented for Brillouin zone sampling. The convergence criteria were set to 0.02 eV/Å for atomic force and 10^{-5} eV for energy, correspondingly. The free energies were calculated using the computational hydrogen electrode (CHE) model. The Gibbs free energy of adsorption ΔG, was calculated following the equations:

$$\Delta G = E_{ads} + \Delta ZPE - T\Delta S \quad \text{.....(S1)}$$

Where, the E_{ads} is formulated as:

$$E_{ads} = E_{slab+adsorbate} - E_{slab} - E_{adsorbate} \quad \text{.....(S2)}$$

ΔZPE stands for zero-point energy change, and ΔS is for entropy change.

Photocatalytic experiments

The photocatalytic ammonia decomposition reaction was carried out in a liquid-solid phase reaction in a quartz reactor tightly sealed by a septum. The reaction was conducted under light irradiation of a 300 W Xe lamp (PLS-SXE300D, Perfect Light) with AM 1.5G filter without the use of any noble metal and sacrificial agents. Typically, 2 mg of the sample was dispersed in 7 ml 1 wt% aqueous ammonia and was sonicated (B2500R-DTH, Branson) for 5 min. The solution was then transferred into a reaction vessel and stirred. Subsequently, the reactor was sealed and purged with pure Ar for 10 minutes to remove air. Finally, the Xenon lamp was turned on to initiate the photocatalytic reaction. Following completion of the photocatalytic reaction, the reactor was allowed to cool, and GC measurements were conducted at room temperature.

For stability testing, after each cycle of 8 hours of reaction, the light source was turned off. The reactor was then degassed again by purging with pure Ar for 10 minutes to remove gases from the previous reaction cycle, and the light source was reactivated to initiate the next reaction cycle.

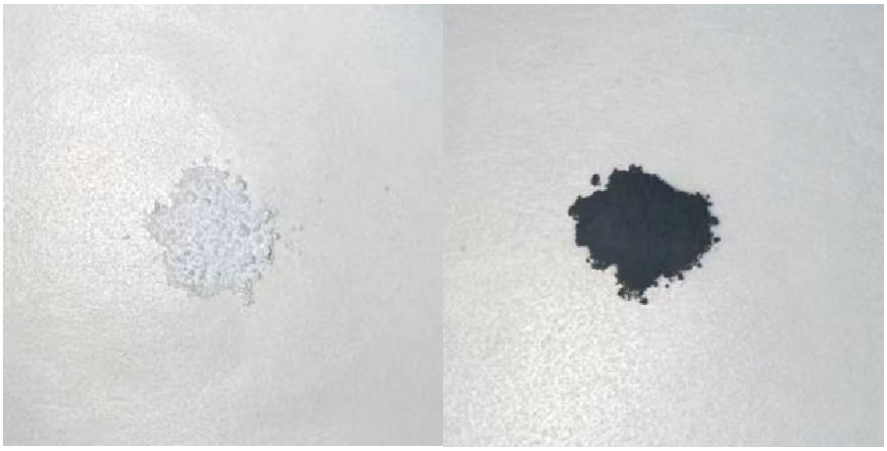

Figure S1. Images of TiO_2 (left) and Ni-NC@TiO_2 (right).

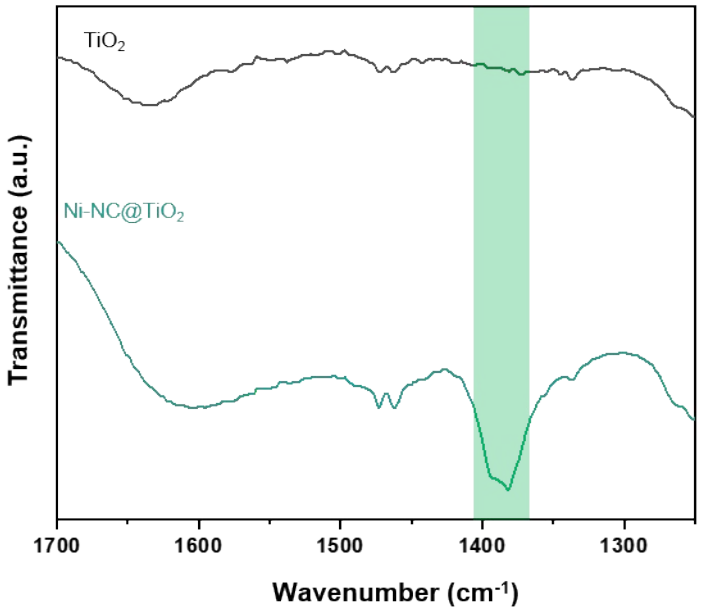

Figure S2. FT-IR spectra of TiO_2 and Ni-NC@TiO_2.

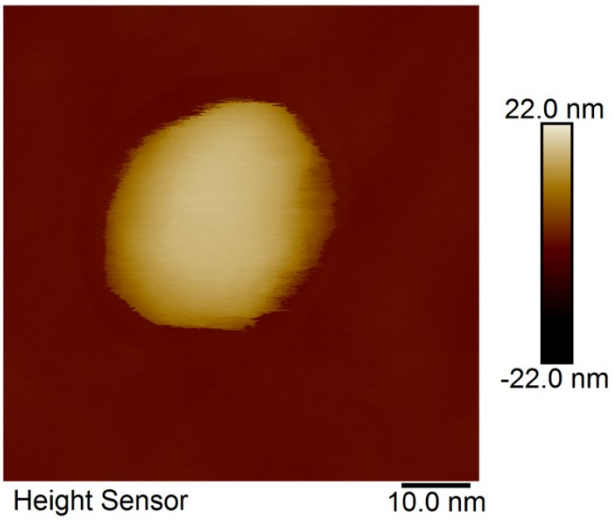

Figure S3. AFM images of Ni–NC@TiO_2, showing a spherical morphology with particle diameters of 20–30 nm.

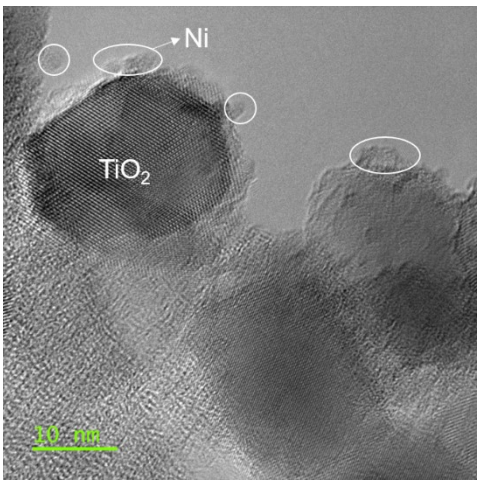

Figure S4. TEM images of Ni-NC@TiO_2.

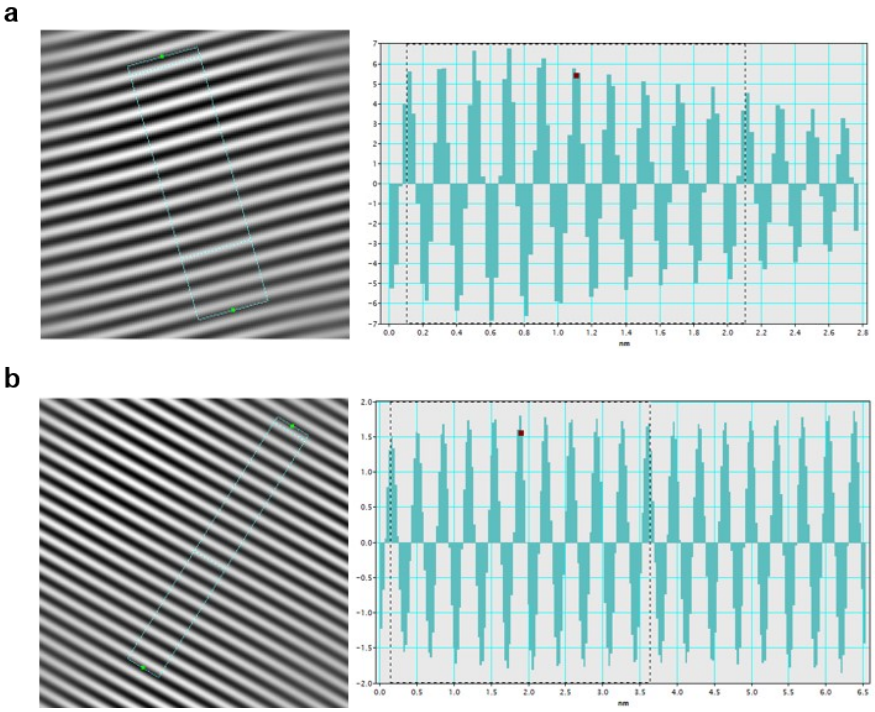

Figure S5. IFFT-filtered images and lattice-fringe line profiles of (a) Ni and (b) TiO_2.

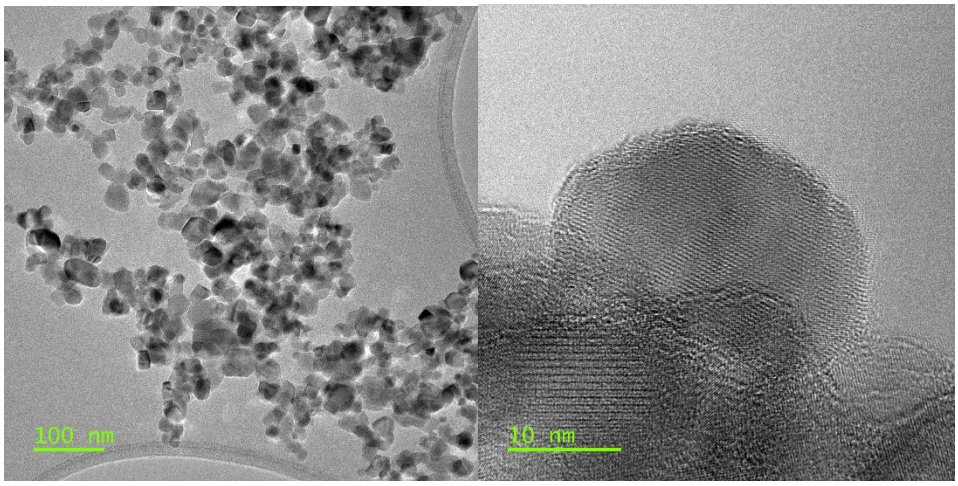

Figure S6. TEM images of NC@TiO_2.

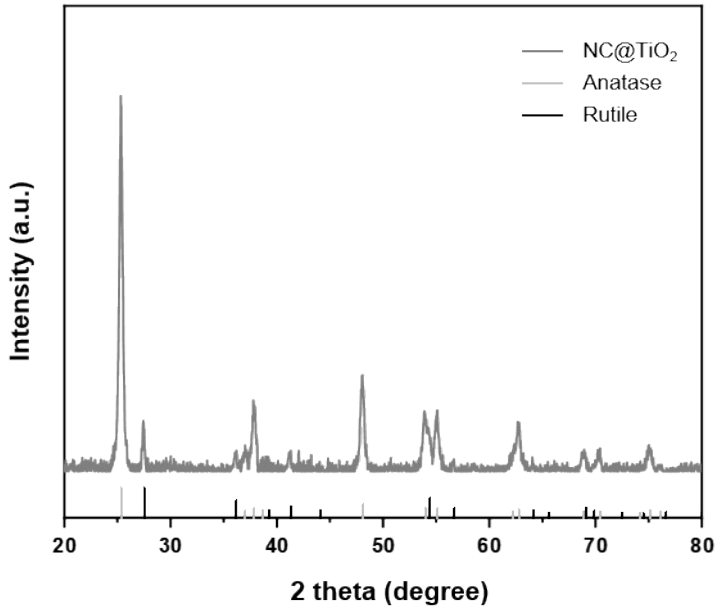

Figure S7. XRD patterns of NC@TiO_2, all diffraction peaks of NC@TiO_2 can be indexed to TiO_2 (anatase and rutile).

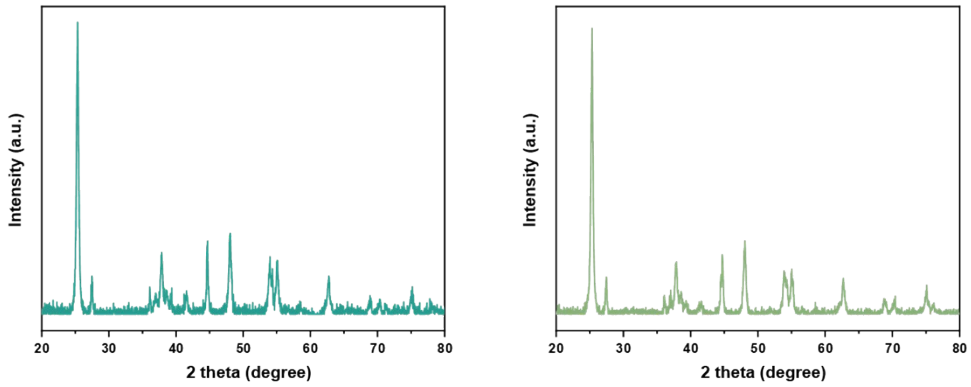

Figure S8. XRD patterns of Ni–NC@TiO_2 before (left) and after (right) the reaction.

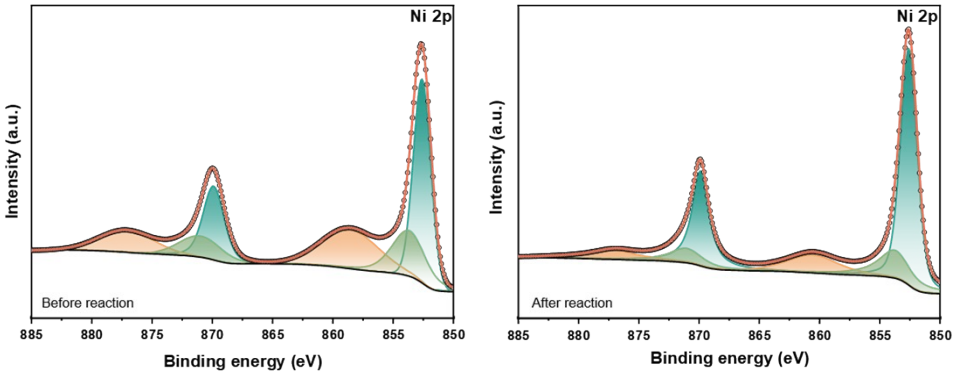

Figure S9. XPS patterns for Ni 2p before (left) and after (right) the reaction.

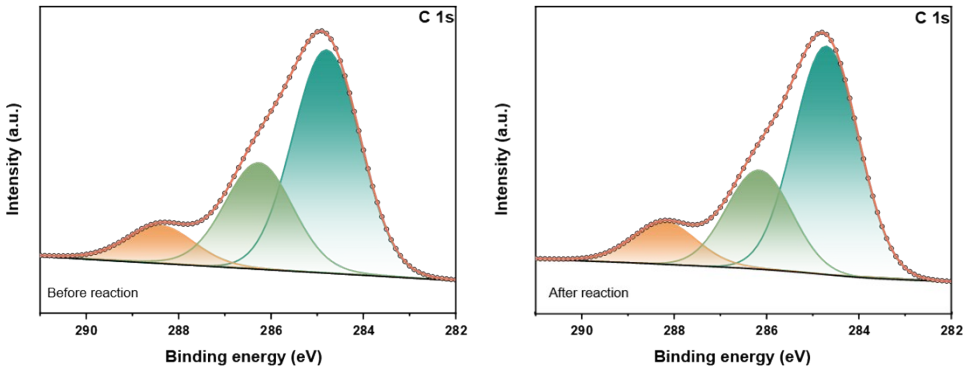

Figure S10. XPS patterns for C 1s before (left) and after (right) the reaction.

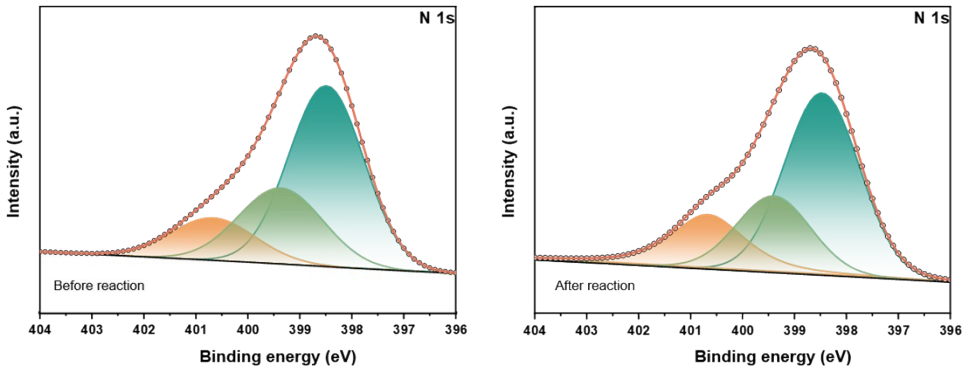

Figure S11. XPS patterns for N 1s as before (left) and after (right) the reaction.

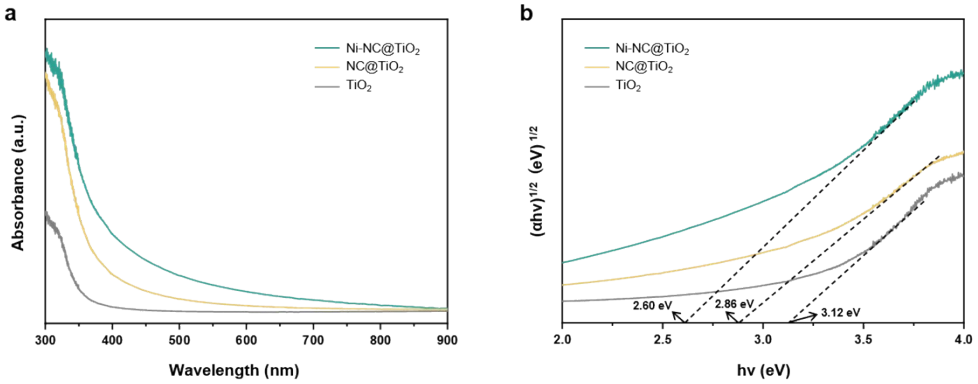

Figure S12. (a) UV–vis diffuse reflectance spectra of TiO_2, NC@TiO_2, and Ni–NC@TiO_2. (b) Corresponding Tauc plots for the determination of the optical bandgap.

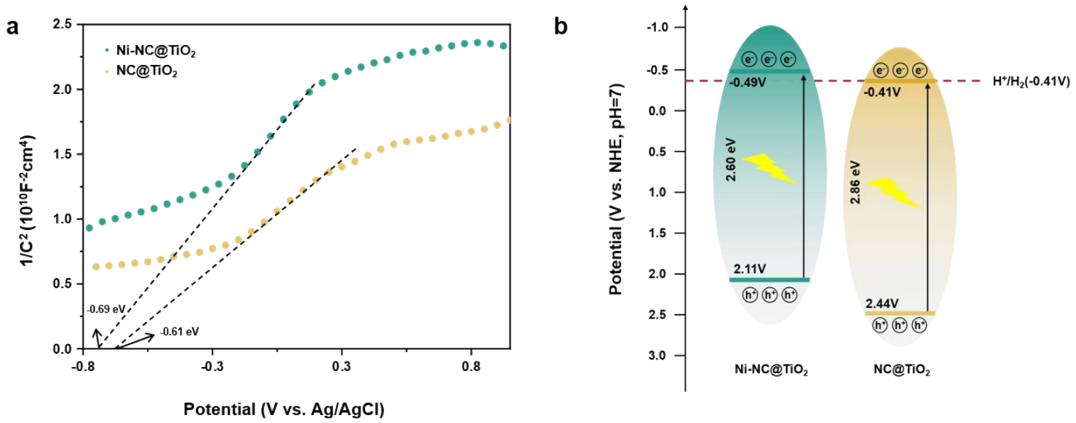

Figure S13. (a) Mott–Schottky plots for Ni-NC@TiO_2 and NC@TiO_2. (b) Schematic diagram of the band structure for prepared Ni-NC@TiO_2 and NC@TiO_2. Here, the conduction band positions shown in panel (b) were estimated from the flat-band potentials derived from the Mott–Schottky plots in panel (a) after conversion from the Ag/AgCl reference scale to the NHE scale using $E_{NHE} = E_{Ag/AgCl} + 0.197\ V$.

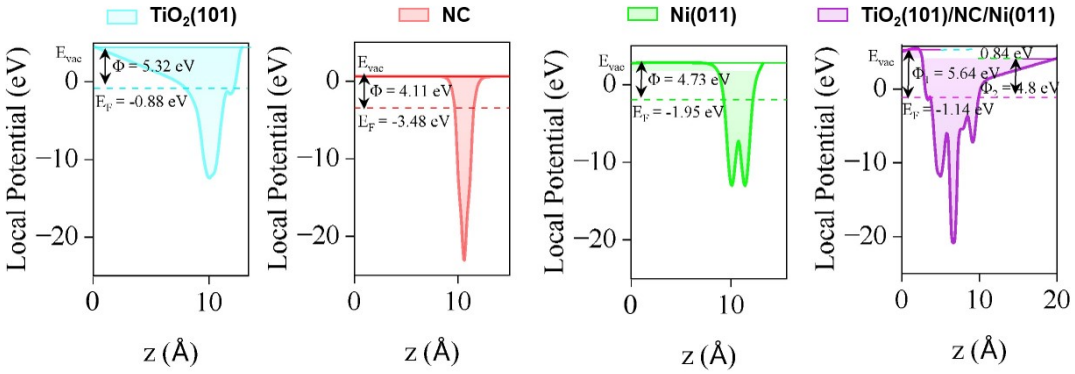

Figure S14. Calculated planar-average local potential for TiO_2 (101), NC layer, Ni(011), and Ni-NC@TiO_2 system.

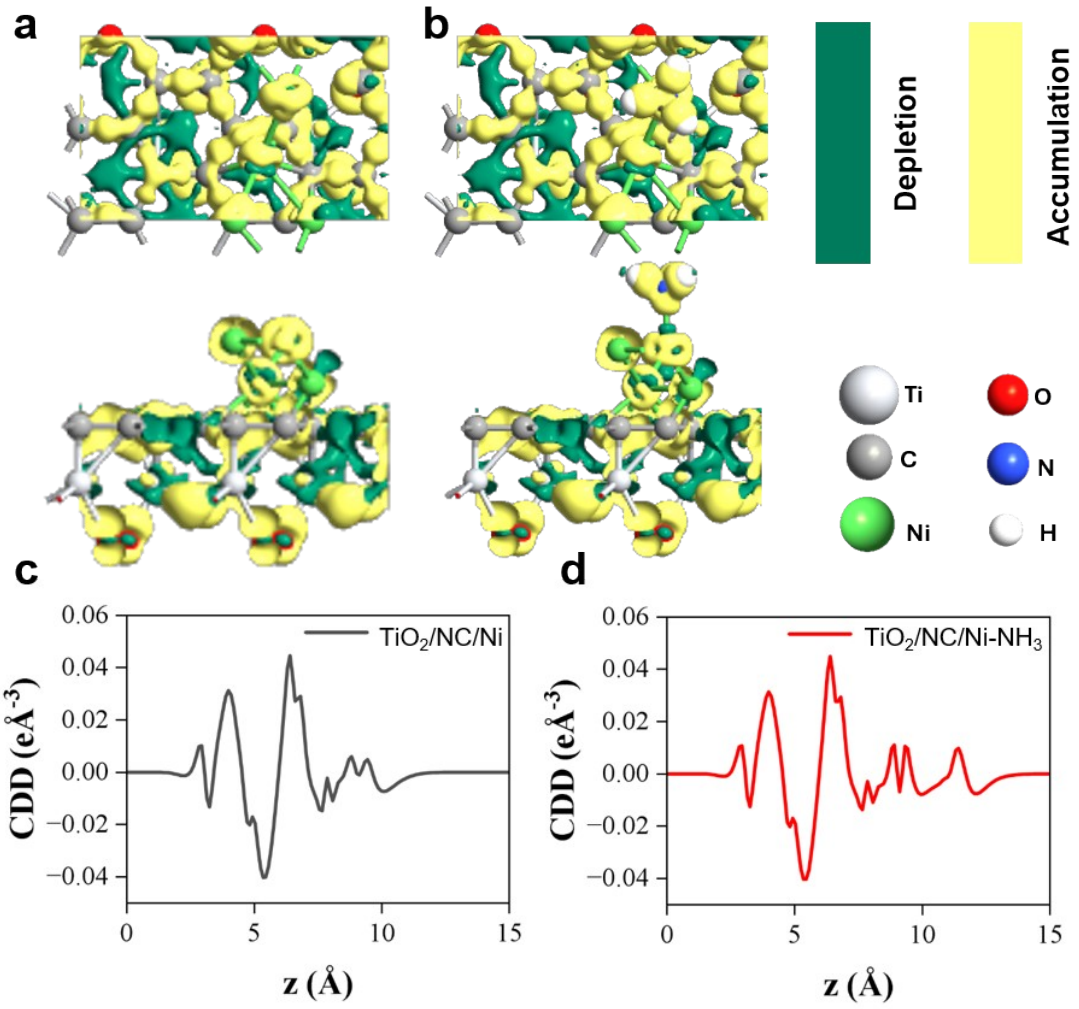

Figure S15. Calculated electron density difference contour of (A) TiO_2/NC/Ni, (B) TiO_2/NC/Ni-NH_3, with iso value (0.001 e/Å^3), electron density line profile of (C) TiO_2/NC/Ni, and (D) TiO_2/NC/Ni-NH_3 system.

Table S1. Summary of TiO_2-Based Photocatalytic Hydrogen Production from Low-Concentration Ammonia Aqueous Solutions (Sacrificial-Agent-Free)

Catalysts	Initial concentration	Production rate μmol/g/h	Reaction time of stability test	Reference citation
Ni-NC@TiO_2	7ml 1wt%	496.75	40h	This work
Pt/TiO_2	5ml 0.1mol/L	450	/	[2]
$Pt_{0.9}Au_{0.1}$/TiO_2	100ml 0.4wt%	285.67	/	[3]
rGO (reduced graphene oxide)/TiO_2 NWs(nanowires)	100 ml 0.883 g/L	208.33	/	[4]
Ce/TiO_2	100 mL, 0.8274 g/L	106	/	[5]
Ni/TiO_2	5 mL, 0.59 mol/L	43.9	/	[6]
Pt(0.5 wt%)-Fe(1.0 wt%)/TiO_2	5 mL, 0.59 mol/L	5.8	/	[7]

Table S2. Summary of TRPL results of Ni-NC@TiO_2 samples.

sample	Excitation-Emission	t1 (ns)	t2 (ns)	t3 (ns)	Average time (ns)
Ni-NC@TiO_2	375nm -420nm	0.63998	5.58286	0.58377	1.08531
NC@TiO_2	375nm -420nm	4.07211	12.2456	0.15397	1.91095
TiO_2	375nm -420nm	7.77761	3.48279	0.24059	2.52139

Table S3. Summary of g-factors of Ni-NC@TiO_2 catalysts.

sample	**g - factor**
NC@TiO_2	2.0043
Ni-NC@TiO_2-L	2.0062
Ni-NC@TiO_2	2.0069
Ni-NC@TiO_2-H	2.0071

Reference：

1 B. Ravel and M. Newville, *Synchrotron Radiation*, 2005, **12**, 537-541.

2 H. Kominami, H. Nishimune, Y. Ohta, Y. Arakawa and T. Inaba, *Applied Catalysis B: Environmental*, 2012, **111-112**, 297-302.

3 Y. Shiraishi, S. Toi, S. Ichikawa and T. Hirai, *ACS Applied Nano Materials*, 2020, **3**, 1612-1620.

4 Z. Wu, N. Ambrožová, E. Eftekhari, N. Aravindakshan, W. Wang, Q. Wang, S. Zhang, K. Kočí and Q. Li, *Emergent Materials*, 2019, **2**, 303-311.

5 M. Reli, N. Ambrožová, M. Šihor, L. Matějová, L. Čapek, L. Obalová, Z. Matěj, A. Kotarba and K. Kočí, *Applied Catalysis B: Environmental*, 2015, **178**, 108-116.

6 A. Utsunomiya, A. Okemoto, Y. Nishino, K. Kitagawa, H. Kobayashi, K. Taniya, Y. Ichihashi and S. Nishiyama, *Applied Catalysis B: Environmental*, 2017, **206**, 378-383.

7 K. Obata, K. Kishishita, A. Okemoto, K. Taniya, Y. Ichihashi and S. Nishiyama, *Applied Catalysis B: Environmental*, 2014, **160-161**, 200-203.